Shahrood University of Technology

Journal of Mining and Environment (JME)

Journal homepage: www.jme.shahroodut.ac.ir

Iranian Society of Mining Engineering (IRSME)

Detection of Karst Features using Integrated Geophysical Methods; Case Study Ravansar Area

Hamidreza Baghzendani[1], Hamid Aghajani[1]*, and Gholam Hossein Karami[3]

1. Faculty of Mining, Petroleum and Geophysics Engineering, Shahrood University of Technology, Shahrood, Iran
2. Geology Department. Kharazmi University, Tehran, Iran

Article Info

Received 26 August 2024
Received in Revised form 8 October 2024
Accepted 20 October 2024
Published online 20 October 2024

DOI: 10.22044/jme.2024.14984.2855

Keywords

Cavity detection
Microgravity
Electrical resistivity
Induced polarization
Karst

Abstract

Karsts are important sources of groundwater, and it is crucial to determine their water volume and quality. The Ravansar Karst spring in the Kermanshah province is a significant water resource with a substantial water volume in the area. The source of this spring is the carbonate rock unit from the Cretaceous period and is affected by tectonic changes and faulting caused by movements related to the Zagros folding. In this work, geophysical methods of microgravity, electrical resistivity, and induced polarization have been utilized to identify the extent of karst development in the limestone units. The minimum residual gravity values are associated with karstification. The field dataset comprised two electrical profiles with the dipole-dipole and pole-dipole arrays. The resistivity and gravity data were inverted using a 2D algorithm based on the least square's technique with a smoothing constraint. According to the processing and 3D modelling of gravity data; not only cavity-shaped voids and spacious cavity chambers were identified but also sub-structures and micro-karstification in carbonate rocks were detected. The most significant finding from the field survey is the detection of low gravimetric values, indicating relatively large holes and chambers that were previously unknown and inaccessible from ground level. These findings are consistent with known collapse and sediment infill features, as seen in surface sinkholes, cavities, and karstification systems. Geophysical surveys and field surveys show that the holes and karsts in the area are related to tectonic phenomena and faulting and are conduits for transporting water to the Ravansar spring.

1. Introduction

In carbonate units where karstification takes place due to atmospheric waters. Over a period of time, air humidity accelerates this process. The internal structure of the karst system is a complex structure with different operators, each of which alone cannot provide the karst creation cycle [1, 2]. In the formation of karsts, limestone rocks are the most important formations, and suitable lithology along with faulting in an area can help to develop or create karsts. Fault networks in the karsts not only feed the karst and create temporary or permanent storage tanks, but also cause the transfer and direction of water to the karst outlets. Also fault systems in karsts affect the shape and geometry of the karst [3]. Geophysics research works, civil engineering, and hydrogeology are three fields that are very interested in the investigation of karst cavities. First, buildings and transportation infrastructure may be particularly affected by subsidence caused by the collapse of karst cavities. The hydrodynamics of carbonate aquifers, which are a significant supply of water in arid and semiarid regions due to their rapid rate of recharge, significant storage capacity, and high quality of water, are also influenced by karst cavities [4].

Karst characteristics commonly arise as a result of chemical breakdown in places with carbonate rocks. Depending on the karstification level such formations are found at various depths,

Corresponding author: haghajani@shahroodut.ac.ir (H. Aghajani)

and have a range of geometries and sizes. Karst formation, subterranean hydrogeological systems, and surface morphology all interact directly and continuously in this kind of environment [5, 6]. As a result, karst systems are exceedingly complex and frequently linked to geotechnical and environmental risks [7, 8].

Because of their size, certain karstic cavities may be directly described and mapped from the surface. many cavities; however, are still separated from the surface or are only connected by tiny cracks. Geophysical methods must be used to indirectly describe these cavities. Each method's applicability range is determined by a physical attribute that is being researched. Strong lateral and vertical fluctuations in the examined physical parameters demonstrate the complexity of karst environments in geophysics. Karstic cracks and cavities can be filled by air, clay, water, or a combination of these. This affects density, electrical resistivity or seismic velocity in geophysical data. A geophysical survey using a combination of at least two approaches is thought to be more trustworthy since any individual physical characteristic can be impacted by a variety of factors [9, 10].

Cavity detection using gravity methods has been practiced since the 1960s [11, 12], and electrical prospecting has been employed since the 1980s [13]. In the more recent times, the emergence of Electrical Resistivity Tomography (ERT) has positioned it as a crucial method for imaging near-surface geological structures including cavity detection [9, 14-27]. The resistivity value is influenced by multiple factors including the presence of karst features found in limestone. ERT has been successfully utilized in diverse geological contexts such as mapping cavities [22, 28-30], identifying water-filled karst conduits [31-33], detecting underground voids in urban areas or prior to significant construction projects [34-37]. ERT has proven to be highly effective in these applications [38]. Cavities, which can contain water, loose sediments, or air, exhibit distinct resistivity values that differ from their surroundings [21, 39, 40]. However, in certain cases, the precise delineation of cavities can be challenging due to exceptionally high resistivity conditions or the presence of a mineral-conductive layer surrounding the cavity [39, 41]. On occasion, small cracks, joints, or fractures like karst features may not be explicitly delineated during the inversion process. Nevertheless, these features can still influence the overall resistivity response, contingent on their size, density, and the material they are filled with. However, a combination of techniques is common for penetration to depths greater than 40 meters under certain conditions. In the case of the combined microgravity and ERT methods, McGrath, Styles [14] effectively documented karstic voids at depths of up to 5 meters. More recently, Gambetta, Armadillo [27] successfully tested the gravity and electrical response to identify a known shallow cave segment situated approximately 30 meters below the ground surface. Furthermore, geophysical surveys such as magnetic and IP-resistivity surveys are extensively employed for probing subsurface properties through the detection of fluctuations in the physical attributes of rocks and minerals. Haritha [42] emphasizes processing and interpretation of magnetic and IP-resistivity data, facilitating the understanding of Earth's-subsurface formations and the identification of potential mineral reserves. The utilization of suitable geophysical methods for data processing, such as data filtering, imaging, inversion, and modeling has been crucial. The outcomes of the data analysis yield valuable insights into sub-surface geology. Mirzaei, Hafizi and Riahi [43] provided a method based on geoelectrical tomography for the precise determination of the water well drilling location in the karstic limestone rocks of Izeh, southwest Iran. The 1D interpretation followed by 2D electrical resistivity and IP tomography in two sites, horseshoe syncline and the west of Izeh limestone, are carried out to propose the best locations for drilling of water wells.

In the studied area, many hydrogeological studies have been conducted regarding the feeding rate of this large freshwater source, as well as its relationship with tectonic discussions, which has been a major ambiguity. In this research work, by utilizing precise geological and tectonic observations alongside depth geophysical data and simultaneous interpretation, an attempt was made to establish a connection between different methods, and ultimately delineate the reservoir shape or water conduit until reaching the spring.

Given the limitations of various geophysical methods, the simultaneous use of multiple methods can enhance the interpretation and accuracy of the findings. The aim of the present work is the interpretation and modeling of a conceptual structure, and pattern of karst that has been done by combining geophysical information such as gravity and electrical resistivity data with geological and hydrogeological data.

2. Methodology

The detection and mapping of subsurface cavities is one of the most common uses of microgravimetry. These cavities can be natural, such as solution cavities found in limestone, dolomite, and evaporite formations, or they may be man-made, like tunnels or mines. Cavities may contain air, water, or secondary geological material. Gravimetry, as a potential field method, is particularly effective for identifying and delineating cavities, which can be challenging to detect using other geophysical techniques[44]. In karst regions, where solution cavities are part of the natural geological complexity, microgravimetry is an essential tool, complementing other geophysical, geological, and direct investigation methods. Electrical methods, on the other hand, have proven especially effective for groundwater and cavity exploration because rock properties significant to hydrogeology such as permeability, porosity, and dissolved minerals are closely related to electrical resistivity. Both electrical and gravity methods detect variations in the physical properties of rocks, which depend on factors such as the rock's matrix, mineral composition, pore structure, and fluid content. These variations result in different anomalies based on the rock's physical characteristics, target size, and depth of burial.

2.1. The electrical resistivity method

The electrical resistivity (ER) method is one of the fundamental geoelectrical techniques used to investigate subsurface structures and identify geological features, based on Ohm's law. In this method, an artificial electrical current is injected into the ground, and the resistivity of the soil or rocks is measured. This process is typically carried out using four electrodes: two electrodes for injecting the current and two other electrodes for measuring the electrical potential difference. By measuring the potential difference, researchers can estimate the resistivity of each subsurface layer. The apparent resistivity is calculated by measuring the potential difference ΔV across electrodes at varying spacings:

$$\rho_a = k\frac{\Delta V}{I} \quad (1)$$

where k is a geometric factor based on the relative positions of the four electrodes, and I is the injected current. When multiple electrodes are used simultaneously, data can be collected across a broader area with probes placed at different depths, ensuring full coverage. To optimize an initial multi-layer model derived from these apparent resistivity values, a fast numerical approach is necessary. This data can then be transformed into a true subsurface geological model using inversion techniques. Methods like finite difference (FD) or finite element (FE) are commonly applied to compute the 2D or 3D forward response of the model. Successive iterations help refine the model until the root mean square (RMS) misfit between the observed data and the model's pseudo-section is minimized. Changes in resistivity usually indicate variations in subsurface materials or pore fluids.

One of the main challenges in this method is the influence of heterogeneity and anisotropy in the composition and structure of the ground. In such conditions, the measured values do not represent the true resistivity of the earth but rather the apparent resistivity, which depends on the characteristics of different subsurface layers. Other factors, such as moisture, mineral types, the presence of specific minerals, and the degree of water saturation, can also affect resistivity. Therefore, when interpreting the data obtained from the resistivity method, it is important to combine the results with other geophysical methods and geological data for more accurate and effective exploration [45].

Moreover, the measured resistivity is influenced by the distance between the electrodes and their geometric arrangement. Changes in the spacing or configuration of the electrodes can alter the distribution of the electrical current and the potential difference being measured. Thus, before taking measurements, the electrode arrangement must be chosen to provide the maximum amount of information about the subsurface structure and minimize geometric effects. These dependencies should be considered in data analysis and interpretation so that the results can provide an accurate picture of subsurface conditions [46].

2.2. Gravity method

The gravity method is used in the studies of changes in the density and mass distribution of the earth's crust. The effective physical parameter used in this method is the density comparison between different geological phenomena and their host rocks. Karstification of carbonate rock units increases the porosity and empty spaces in the rock, and subsequently decreases the density of the rock unit. This phenomenon causes a significant increase in the , which can be measured by gravimetry, and is of great importance in the studies of karsts [14].

The gravity method in geophysics measures difference in Earth's gravitational field at specific locations, which are influenced by the properties of the underlying rock masses. This method is particularly effective for near surface cavity exploration in areas where poorly consolidated/unconsolidated low-density rock overlies denser basement or other carbonated rocks. Since gravity is directly proportional to mass, differences between the densities of two rock masses result in noticeable anomalies in the Earth's gravitational field. When these anomalies are accurately measured, they can provide an estimate of the thickness of the unconsolidated rock layer. In regions with crystalline rock, unconsolidated rocks often serve as groundwater aquifers due to their high porosity, permeability, and transmissivity. The bulk density of a fluid-saturated rock is defined as:

$$\rho_{sm} = \rho_r(1-\varphi) + \varphi \quad (2)$$

Mass of the rock, $m = \rho_{sm} v$ where ρ_r is the density of the rock, ϕ is the porosity, and v is the volume.

The gravitational effect, F of the earth on such rock can be defined as:

$$F = G\frac{mM}{R^2} \quad (3)$$

Where M and R are the mass and radius of the earth respectively, G is the universal gravitational constant, and m is the mass of the rock. As the mass of a rock increases, the gravitational influence also increases. The karstic carbonate rocks, due to their high porosity and permeability, are potential aquifers for groundwater. These rocks generally have lower density, resulting in lower gravity readings compared to denser rock types.

Gravity data for each study is typically collected on grids or profiles, depending on the survey's scale and the target's size, using a high-precision gravimeter. During data collection, a base station is set up. The field crew regularly returns to this base station to record gravity measurements at specified intervals to account for tidal effects on gravity values. Observed data is usually corrected for instrument drift and tidal effect. In addition to this, the data is subjected to normal gravity, free-air correction, bouguer correction and terrain correction. Bouguer gravity anomaly, ΔgCB can be described as:

$$\Delta g_{CB} = (g_{obs})_{ABS} - g_\phi + \delta g_{FA} - \delta g_B + \delta g_T \quad (4)$$

Where $(g_{obs})_{ABS}$ is the measured data (after transformed to absolute gravity) on each station, g_φ is normal gravity, δg_{FA} is the free air correction, δg_B is the bouguer correction, and δg_T is the terrain correction [47]. Figure 1 shows the effect of gravity corrections on gravity data.

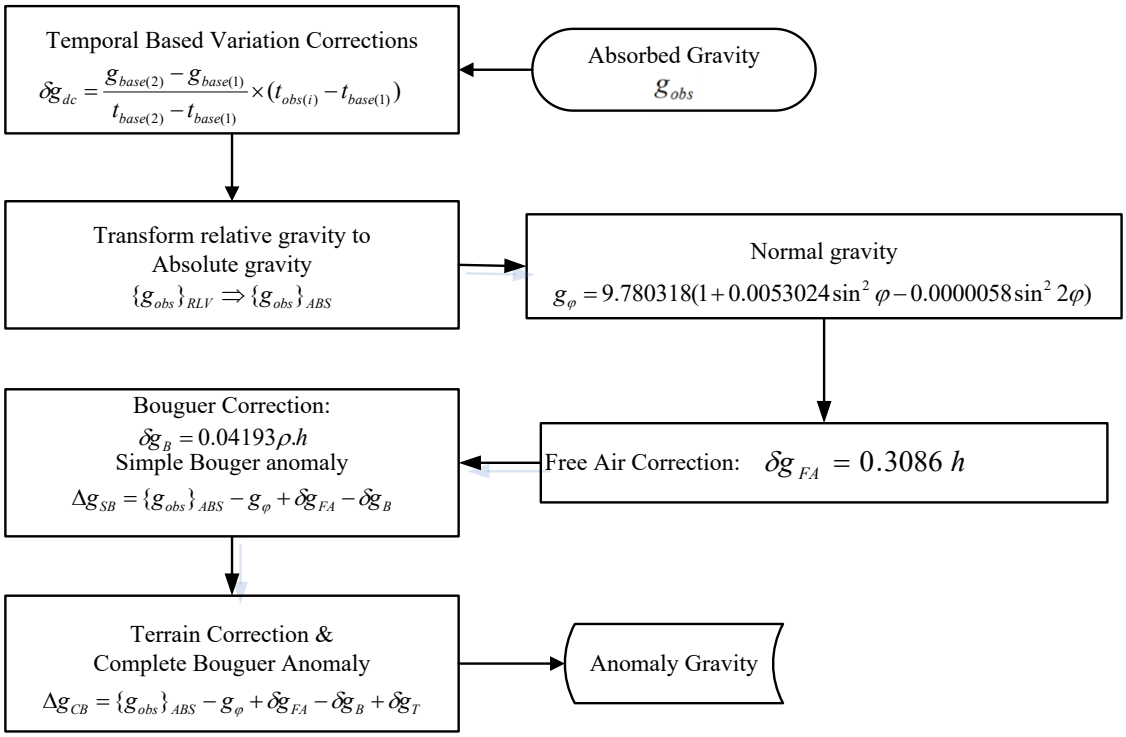

Figure 1. Calculation of gravity anomaly (complete Bouguer)

2.3. Gravity inversion

In geophysics, the purpose of finding a solution to an inverse problem is to calculate the parameters of the Earth's sub-surface using just a limited set of geophysical measurements as the input. An approximate approach for the solution of the ill-posed inverse problem can be achieved by minimizing the objective function [48-50]:

$$\varphi(m) = \varphi_d(m) + \lambda\varphi_m(m) \quad (5)$$

The m parameters of the Earth model are included within the vector of m, the value of the data misfits is denoted by the symbol$\boldsymbol{\varphi_d}$, whereas a value of some attribute of the density model is denoted by$\boldsymbol{\varphi_m}$. The regularization parameter $\boldsymbol{\lambda}$balances the impacts of $\boldsymbol{\varphi_d}$ and $\boldsymbol{\varphi_m}$in the objective function. Here we assume the linear inverse problem in which the data vector $\boldsymbol{d}$and the unknown parameters are related by $\boldsymbol{Gm} = \boldsymbol{d}$, where$\boldsymbol{G}$ is the kernel matrix with $\boldsymbol{N}$ by $\boldsymbol{M}$size. We calculated the elements of the kernel matrix by the formula given by Blakely [51]. Furthermore, We took it for granted that the measured data's noise was unrelated to one another and Gaussian with a standard deviation of $\boldsymbol{\sigma_i}, \boldsymbol{i} = 1{:}\,\boldsymbol{N}$; for the ith measured data point in the observed data vector $\boldsymbol{d^{obs}}$.Then defining the inverse square root of the data weighting matrix to be $\boldsymbol{W_d}$ the noise in the data is whitened by applying the matrix $\boldsymbol{W_d}$ to both $\boldsymbol{G}$,and $\boldsymbol{d^{obs}}$,and the data misfit was measured by the weighted norm as follows:

$$\varphi_d(m) = \left\| W_d[d^{obs} - Gm] \right\|_2^2 \quad (6)$$

$$W_d = diag\{\frac{1}{\sigma_1},...,\frac{1}{\sigma_N}\} \quad (7)$$

In the following discussion, we implicitly assume that the whitening transform has been applied and now refer uniformly to $\boldsymbol{G}$ and $\boldsymbol{d^{obs}}$ as the weighted matrix and vector, respectively. Generally, $\boldsymbol{N} < \boldsymbol{M}$, and the discrete inverse problem is underdetermined [48, 50]. Therefore, the final model, which is known as an acceptable model in this inversion method, is a model in which the value of the function$\boldsymbol{\phi_d}$ is minimum.

For stabilization, there are countless possibilities for incorporating prior information on the model. Here we considered the use of the smoothing norm:

$$\varphi_d(m) = \left\| Gm \right\|_2^2 \quad (8)$$

where **C** is an estimation of the second-order derivative operator that is called a regularization matrix. Practically, in the inverse modeling of potential field data, it is recognized that the non-zero model parameters concentrate near the surface of the modeling domain. This problem is alleviated by applying a depth weighting matrix.

$$W_z = diag\{\frac{1}{(z_1^{\beta}},...,\frac{1}{z_M^{\beta}}\} \quad (9)$$

where $\boldsymbol{z_j}\,;\boldsymbol{j} = 1{:}\,\boldsymbol{M}$ is the mean depth of subsurface cells. Then in Eq. 8, $\boldsymbol{C}$ is replaced by $\boldsymbol{CW_z}$. For the inversions considered here, we selected $\boldsymbol{\beta} = 1$, and as with $\boldsymbol{\phi_d}$, we now uniformly use $\boldsymbol{C}$ in the stabilization function $\boldsymbol{\varphi(m)}$ along with the weighting matrix of $\boldsymbol{W_z}$.

By minimizing the objective function in Eq. (5), we calculated $\boldsymbol{m_\lambda}$ as the solution of the inverse problem for a specific $\boldsymbol{\lambda}$. Also, to solve the inverse problem and calculate the kernel matrix, we applied the LSQR method to find the solutions of any linear system of equations before putting the solutions to other equations. Practically, finding a suitable choice for $\boldsymbol{\lambda}$in Eq. (5) is non-trivial. When $\boldsymbol{\lambda}$is large, the effects of the regularization are more robust, and the solution is likely to be resolved, poorly. But with small $\boldsymbol{\lambda}$, the problem may be unstable. Finding a reasonable balance that provides stability and sufficient resolution is usually addressed using a parameter estimation approach. Some approaches are briefly discussed in the following sections. In this research work, the GCV method was used to obtain the λ value. The smoothness constraint to minimize the objective function is widely used in linear inverse problems. In fact, the operator of the second derivative of the model parameter vector is called the smoothing matrix in the objective function. The adjusted least squares solution of the inverse problem is obtained by first-order Tikhonov regularization as follows [52]:

$$\min\left\| Gm - d^{obs} \right\|_2^2 + \beta\left\| Lm \right\|_2^2 \quad (10)$$

$$G^T G + \beta L^T L)m = G^T d^{obs} \quad (11)$$

In Tikhonov regularization, the second order is as follows:

$$L=\begin{bmatrix}1 & -2 & 1 & 0\,0 & 0 & 0 & 0\\ 0 & 1 & -2 & 1\,0 & 0 & 0 & 0\\ 0 & 0 & ..... & ....0 & 0 & ..... & ....\\ 0 & 0 & 0 & 0\,0 & 1 & -2 & 1\end{bmatrix} \quad (12)$$

2.3.1. GCV criterion

The GCV technique is a prevalent approach to find $\boldsymbol{\lambda}$ based on a leave-one-out cross validation procedure [53-56]. A good approximation of $\boldsymbol{\lambda}$ is one that establishes the data without being too dependent on any variable, and minimizes the $\boldsymbol{GCV}$ function [53, 57].

$$GCV(\lambda)=\frac{\left\|d^{obs}-Gm_{\lambda}\right\|^2}{\{trace[I-G(G^TG+\lambda C^TC)^{-1}G^T]\}^2} \quad (13)$$

It is important to note that using this approach requires no prior knowledge about the noise of the data.

3. The Geology of studied area

The scope of the research covers the boundary between latitude $34^{\circ},48^{'},11.68^{''}N$ to $34^{\circ},50^{'},11.03^{''}N$ and longitude $46^{\circ},36^{'},56.65^{''}E$ to $46^{\circ},37^{'},25.96^{''}E$ in the northwest of the Ravansar city in the Kermanshah province.

3.1. The geology map

Most of the available rock units in this area are Jurassic carbonate rocks, and in some areas, these limestone units are divided into three parts, and, as we know, karst development is also related to limestone units (Figure 2). The effect of tectonic factors and weathering on the lithology of the upstream parts of the spring, and has led to an increase in porosity and empty spaces with many regular and irregular cracks and crevices. There are many karstic caves in the limestones of different parts of the Biston Mountain range, and one of the features of karstification of the carbonate rocks of the studied area is the presence of sinkholes, large dimples, and pits (Figure 3).

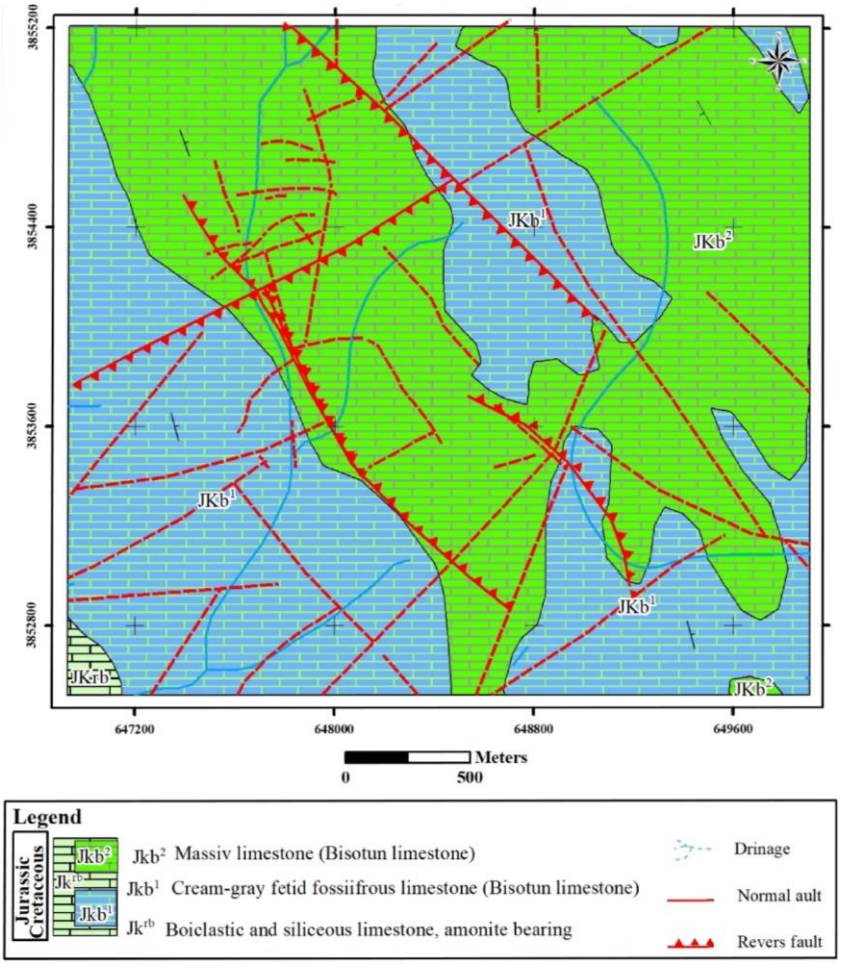

Figure 2. Geological map of the Rvansar spring.

Figure 3. Karstification signs (dimples, pits and cavity) in the studied area.

3.1. Tectonics setting in the studied area

The Shahu Mountain is located in the sedimentary structural zone of the Zagros overthrust. Limestone rocks with thick layers or in the form of a mass in the Biston have high rocky peaks due to bearing the tectonic pressures and drifts created in them. This rolling belt has the highest amount of elevation at a height of more than 2400 meters. The Shahu Mountain has higher peaks compared with other geological units of the Zagros. In the highlands located in Ravansar and Shahu, in addition to the main thrusts caused by the Zagros; the main and subsidiary faults with a northwest-southeast extension as well as transverse faults with a north-south extension have influenced the limestone layer (the Biston), which is a large carbonated piece from the Mesozoic era in the region (Figure 4).

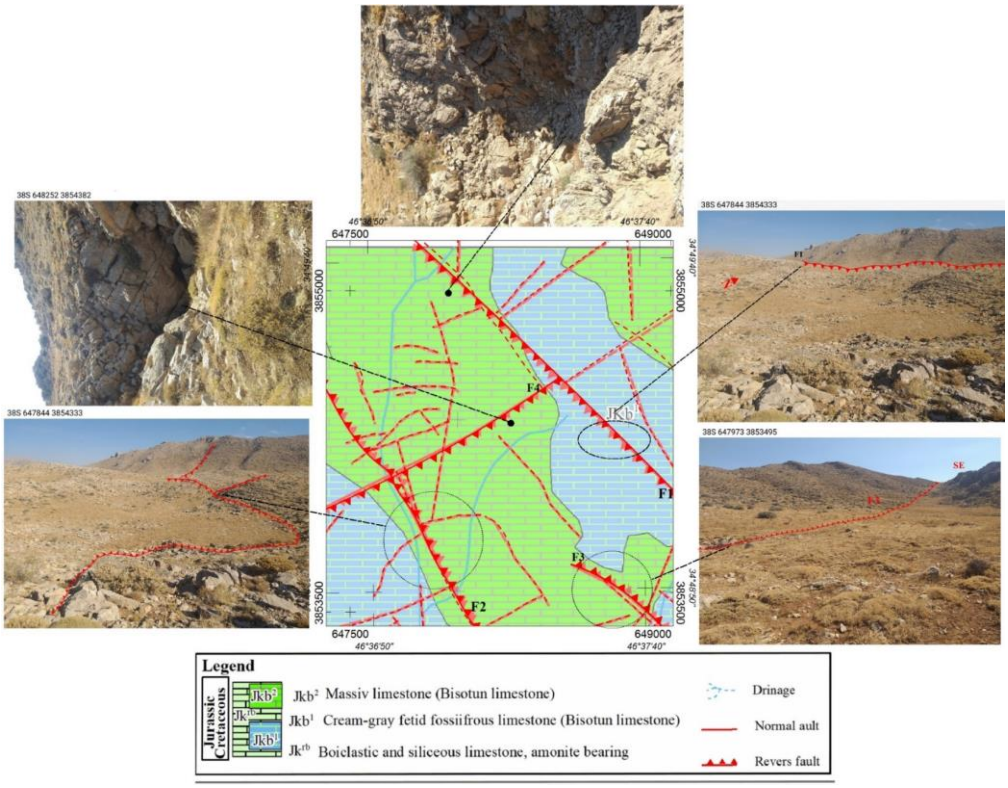

Figure 4. Fractures, cracks, and fissures in the studied area (red line on photo).

Due to the compact structure and the microlithic texture result from the stress and shear forces that have been imposed from different directions (alpine orogeny), the Biston limestone mass has many cracks and fractures (small and large). The geological activities in this area have led to the creation of so many fractures. The frequency and intensity of these fractures and the apparent disorder leading to the syncline or anticline folds in the region cannot be easily recognized (Figure 4). The sinkholes formed along the layering level have the structural trends of the Zagros overthrust that is northwest and southeast. In addition to the faults, the seam and fissure system is well visible in the limestone rocks of the region.

The formation of these joint fissures is not only affected by the fractured geological structure of the region, it is also related to the nature of limestone rocks. Due to the inflexibility of the carbonate formations in the presence of tectonic phenomena, these formations have been severely faulted, and caused a secondary fissure system to develop in them, which has subsequently created important water sources (karstic) in this area.

To assess the condition and function of the faults in the scope of the study, a map of major and minor faults was prepared (Figure 5). Based on this map and the analysis of the results on the Rose diagram, the main trend of the faults is in line with the general trend of the northwest-southeast Zagros zone (extension of 150 or 330 degrees). Also due to the influence of the main faults, a series of faults can be seen in the direction perpendicular to them that is the northeast-southwest trend of about 50 to 60 degrees. The studies conducted on the performance of faults with the mentioned trend indicate the existence of a thrust reverse component from the northeast to the southwest [58].

Field observations show that the morphology and topography of the earth along these fractures confirm the presence of a tensile component. The position of the measured layering indicates the general northwest-southeast extension and the northeast slope direction. In some parts, the direction of the slope is toward the southwest, which is mainly the result of the activity of reverse faults and overthrust. The angle between the fractures along the northwest-southeast layering as well as the thrust direction within and between the rock units, indicate the existence of a compressive force in both the northeast-southwest and east-west directions.

The surface distribution of the effect of fractures and the geometric relationship between them indicate the existence of different stress in the studied area, which has created a complex network of fractures with a high density. Based on the geometrical and spatial relationship between fractures and limestone units inside, and intrusive units outside the studied area, it can be concluded that these two processes have the greatest contribution in controlling magmatic fluids and precipitation. It seems that the most important conduit or natural channel of fluids between different rock units is mainly through the fractures with a northeast-southwest extension. In order to better understand the relationship and impact of faults in creating sinkholes and karstification of the carbonate unit; a map of the density and concentration of faults in the studied area was prepared (Figure 5). According to the findings of the fault density map and field surveys, the main sinkholes and the dimples are in the place where the faults are concentrated [59].

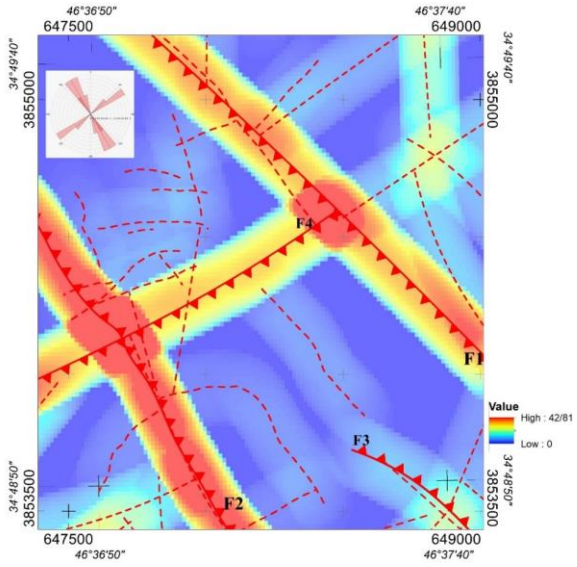

Figure 5. Density map of faults and the rose diagram showing the distribution of faults in the studied area.

4. Data collection and analysis

In this study, to investigate the sub-surface structures caused by the impact of faults, and the karstification process in the studied area, the gravity values were measured on 1700 stations in 28 profiles in a regular network ($50 * 25m$) using a CG5 gravimeter (Figure 6). In this work, We used the first station of the first profile as a local reference point (Local Base station) to perform temporal based variations (instrument drift and tidal effects). For this purpose, measurements were taken again at this Local Base at approximately 3-

hours intervals. Also here, by using absolute gravity-based points established in a regular global and national network with specified intervals, the absolute gravity values of all stations in this area can be calculated. In this case, it is necessary to determine the absolute gravity value of the Local Base station relative to an absolute reference station with a known absolute gravity value. Around the studied area, there are two geodetic Base stations, and we used the Base station that was named 2205, and its absolute gravity was 979321.235 mGal. Necessary corrections were made on the gravity data including drift correction, latitude correction (normal gravity), free air correction, Bouguer correction, and terrain correction, which is shown schematically in the Figure 1. Mapping with the UAV technology and the Dual-frequency Global Positioning System (DGPS) was used to determine the values of the topography effect on the gravity data.

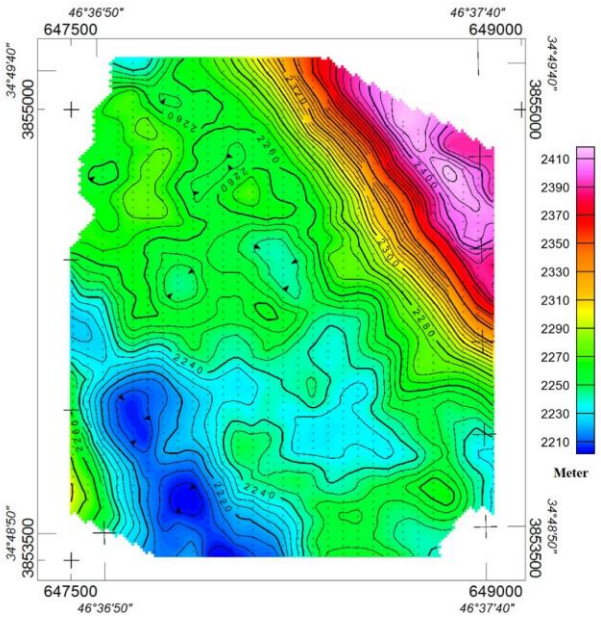

Figure 6. Location of gravity stations on topography map.

By removing disturbing effects and necessary corrections on the gravity data, the *complete Bouguer gravity* values were calculated on each station and then the complete Bouguer gravity anomaly map of study area was drawn (Figure7a). Based on this map, the increasing trend of gravity values can be seen from the southwest to the northeast extension perpendicular to the main stretch of the Zagros. To assess the effects of the surface anomaly caused by the presence of sub-surface karstification structures of the carbonate rock unit in the studied area; it is necessary to calculate residual gravity anomaly on each station. The observed gravity anomalies are the sum of gravity effects of density contrast at various depths in the subsurface half space. In order to studying a specific geological phenomenon using gravity data; the target anomalies must first be separated from the observed gravity anomalies. We calculated regional gravity anomaly in two ways; trend surface and the upward continuation methods [60, 61]. After subtracting this value from the corrected data (observed data), the residual anomalies were calculated (Figure7b).

Since the complete coverage of the area is from one rock unit, which is Biston limestone, the changes in the data and the residual anomaly map can be related to possible karsts or structures that are effective in karst development. The amount of gravity field changes on the residual anomaly map is in the range of -0.16 to +0.14 mGal, and the values in the range of negative anomaly are between -0.160 to -0.001 mGal (indicating the decrease in density caused by the increase in the porosity of the rock unit).

According to Figure 7b, the decreasing changes of residual gravity anomalies with the northwest-southeast trend indicate empty spaces or cavities that can be suitable places for feeding or reserving water in possible karst aquifers. In ground assessments, a lot of evidence of destroyed karsts, sinkholes, and groove and parallel fractures related to faulting have been observed, which is consistent with the results of gravity data. In the central parts, the range of changes in the gravity data (field) was increasing to some extent, but due to the uniformity of the lithology, not many changes were observed in the data. In the field surveys, limestone units with almost horizontal layering have been observed in these sections, which have fewer fractures than the southern sections.

In this area, in order to identify the sub-surface structures, the electrical resistivity data and induced polarization data along to two profiles were measured. The GDD 3600 device was used to collect the electrical data. To achieve proper sub-surface and depth resolution; at the same time, the dipole- dipole and pole-dipole arrays were used to measure the data (general arrays) [62].

The profiles taken in the southern part of the studied area, based on geological field observations, fully align with the trend of faulting and tectonics in the region. However, the northern profile required further investigation due to geological surveys and incremental changes observed in the gravity field. Based on the geological evidence, and the presence of holes,

grooves and sinkhole, electrical data was collected on two profiles along N10E and N60E to investigate the role of factors influencing the development and identification of karst-based resistivity and gravity data (Figure 8). For modelling of data, topography correction was done and then the smoothing inversion method of the data was done using the RES2inv software. In the interpretation of the results of the data, sections with electrical resistivity and inductive chargeability have been used.

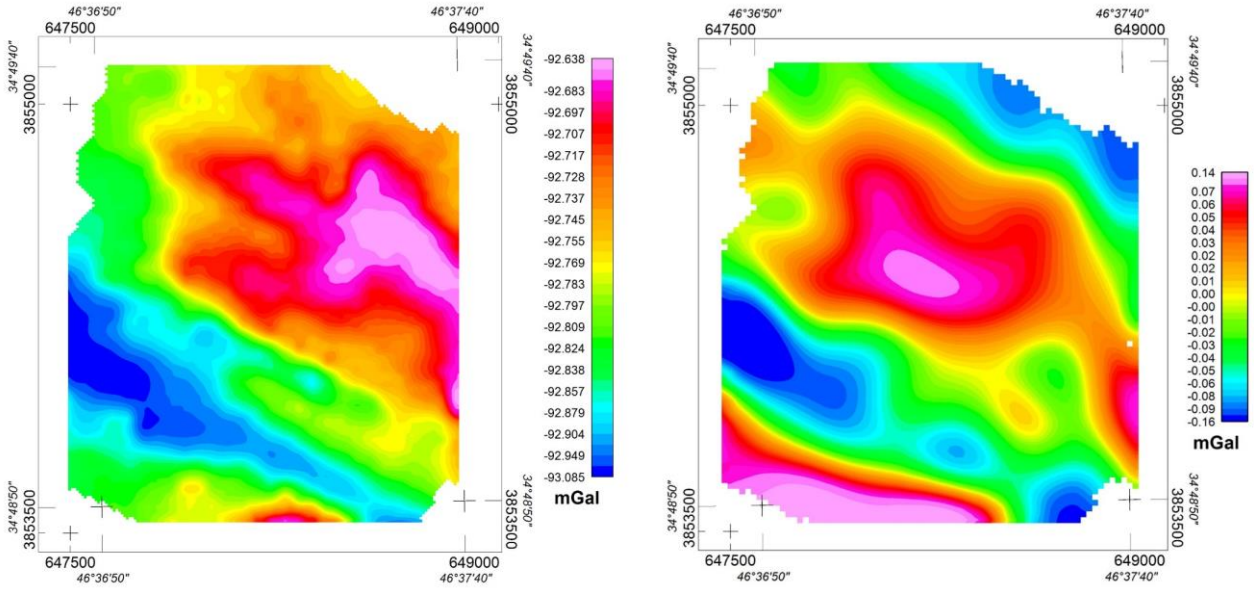

(a) **(b)**

Figure7. The complete Bouguer gravity anomaly map (a) and Residual gravity anomaly map (b) from the studied area.

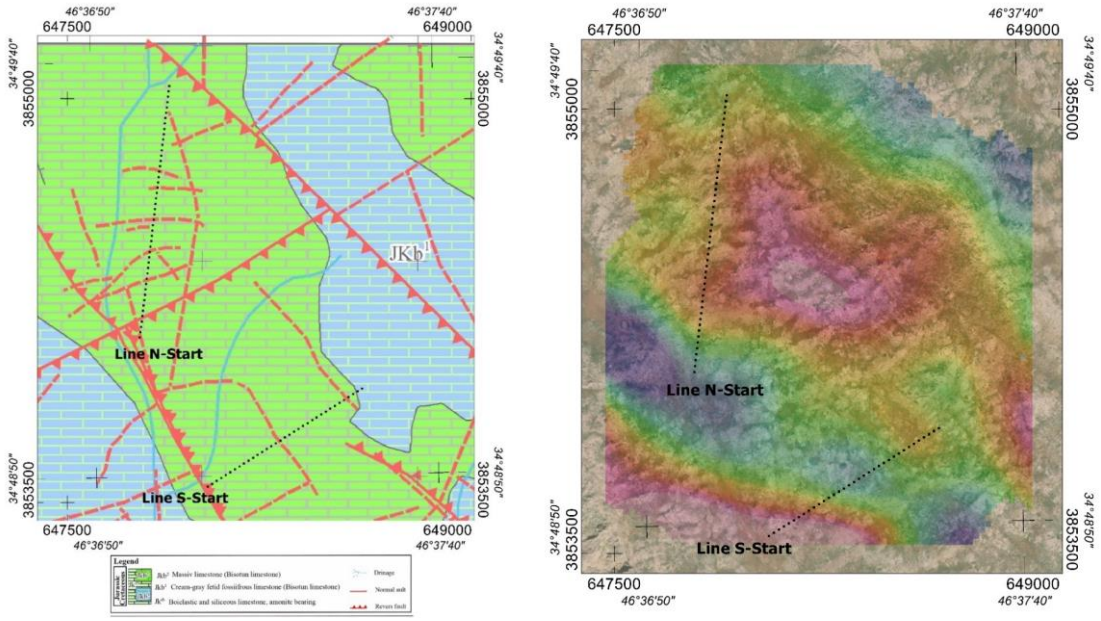

Figure 8. The direction of two profiles to collection electrical resistivity and induced polarization data: on the residual gravity anomaly map (right) and geology map (left).

Based on the method mentioned above, 3D inverse modeling of the gravity data was done using the smoothing inversion method (Figure 9). According to Figure (9), similar to the residual anomaly map, a large and broad negative anomaly can be seen in the southern part of the area, which indicates a sharp decrease in density and an increase in porosity, that these items mentioned during the field visits were confirmed. This anomaly corresponds to the position of the holes in

the area, which are sometimes visible up to the ground level.

To assess and simultaneously interpret the results of the modeling of gravity data and electrical resistivity, two gravity profiles (vertical sections) were prepared from the location of the electrical resistivity profiles, based on the results of inverse modeling of the gravity data (Figures 10C and 11C). According to Figure (10C), the changes in the density comparison in the southern part of the profile are negative, which indicates the presence of holes and empty spaces at a distance of about 200 to 500 meters from its starting point, and it is consistent with the field evidence. Also, in Figure (11C), in the middle of the profile, the amount of gravity changes is decreasing, and the density anomaly is also negative. This is a sign of increased porosity in carbonate rock, which has a decrease in density compared with the surrounding environment, this porosity is controlled by faults and structures. The position of this sub-surface structure is about 200 to 450 meters from the starting point of the profile. In field observations, this position was associated with subsidence in the rock unit, which confirms that.

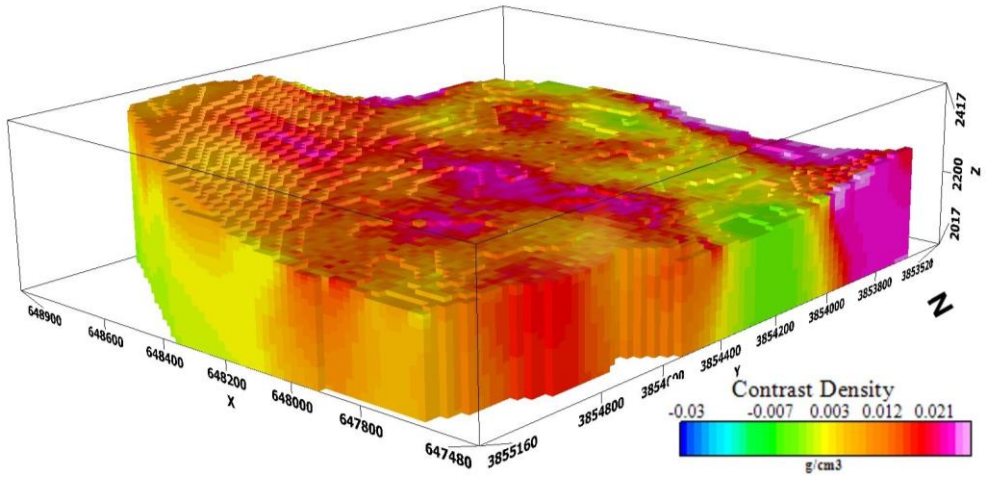

Figure 9. 3D inverse modelling of gravity data in the study area.

5. Interpretation of the Results

5.1. The results of electrical methods on the northern profile (N)

After correcting the topography on the electrical data, smoothing inversion of the data was done using the RES2inv software (Figures 10a and 11a). Based on Figure 10a, the changes in the dip of the stratification are clearly visible on both sides of the electrical cross-section, with the stratification dip initially inclined towards the center of the profile at the beginning of the line and also inclined towards the center at the end of the line. This is also confirmed in the section prepared by the gravity method. In the central part of the geoelectrical section, we observe positive changes near the surface and decreasing changes in electrical resistivity at greater depths, both of which are accompanied by decreasing density changes in the center of the profile. The decreasing density changes are associated with subsurface cavities, and the decreasing changes in electrical resistivity simultaneously indicate the presence of water in this area, which is surrounded by limestone sections.

The decrease in resistivity continues below the stations at 400 meters, which indicates the state of the horizontal structure. This decrease in resistivity in the gravity center section is met with medium to low density in the center, suggesting a structure with more porosity than its surroundings. The large observed in the gravity profile on the left side, i.e. around the stations at 20 to 80 meters, shows the high density of the carbonate formation, which was apparently affected by the higher surface part of the limestones. The deeper parts below the horizon of 2200 meters were more porous.

In the inductive chargeability section, the position corresponding to the decrease in resistivity is associated with a relative increase (although at a low level) of chargeability, which to some extent indicates an increase in porosity that can be saturated by fluid. In the middle part of the profile, the increase in chargeability is associated with an increase in electrical resistance, and it seems to be caused by the special structure of the carbonate unit, and the presence of several faults in the dense and crystalline limestone unit has caused relative chargeability.

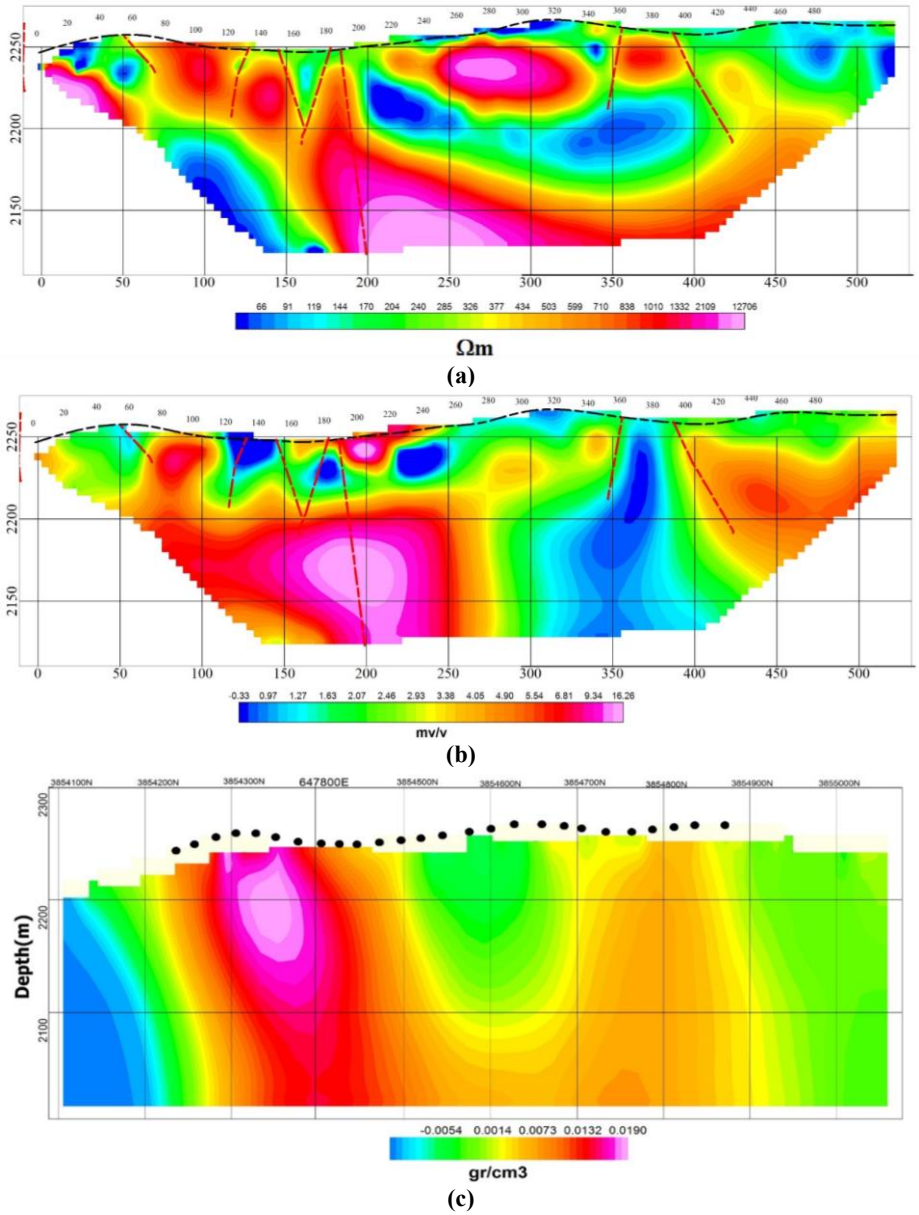

Figure 10. (a) Section results from the inversion of electrical resistivity data on the northern profile; (b) section result from the inversion of inductive chargeability data on the northern profile; (c)the result of inverse modeling of gravity along with the northern profile.

Faults or fractures around the stations 140, 160, 180, 240, 300, and 400 can be easily distinguished. It seems that under the stations 360 to 400, due to the operation of faults, there is a unique environment with a very low amount of charge, which has created a vertical channel that extends to the depth. In the section of resistivity, in its middle part, it has been associated with a decrease in resistivity, and in the gravity section, it is associated with average density.

As a result, it seems that the presence of empty spaces is caused by the development of the karst network, which is sometimes saturated by water fluid. These are the possible locations of sinkholes and fluid passages which were dry at the time of data collection and had a relatively high resistivity. There is an increase in electrical resistivity in the range of 200 to 420 meters, which is interrupted by multiple faults, indicating vertical displacements. The high values of resistivity and density Simultaneously indicate the high density of carbonate rock, which has a small amount of charge, but in the eastern part, it is associated with a sharp decrease in charge, which indicates the crushing and changes in the rock type.

5.2. The results of the electrical methods on the southern profile (S)

Compared with the northern section, the electrical resistivity section in the southern profile

has a smaller range of changes. In this part of the studied area, more evidence of karst development could be observed. There is a blocked pit with low density changes in the vicinity of this section. These changes in gravity modeling are about -0.1 g/cm^3. The electrical resistivity is low from the beginning of the profile to a distance of 140 meters, and continues almost to the depth of about 30 meters. But the increasing trend of resistivity is observed with increasing depth of current penetration. Based on the electrical and gravity data, this area is separated from the next section by a relatively deep fault (at a distance of 160 meters from the resistivity section), and the decrease in density indicates an increase in empty space and a greater porosity than the surrounding environment. Its deep and horizontal expansion (in the direction of the section) is high and its corresponding limits on the chargeability section indicate a relative increase in chargeability compared with the surrounding environment, and probably contains fluid with lime salts. The increase in the value of resistivity in this part of the cross-section as much, as 400 milliohms cannot be attributed only to the presence of voids or porous spaces without water. Based on the chargeability section and the decrease of the density in the gravity modeling section, it indicates the presence of karst containing water (figure11).

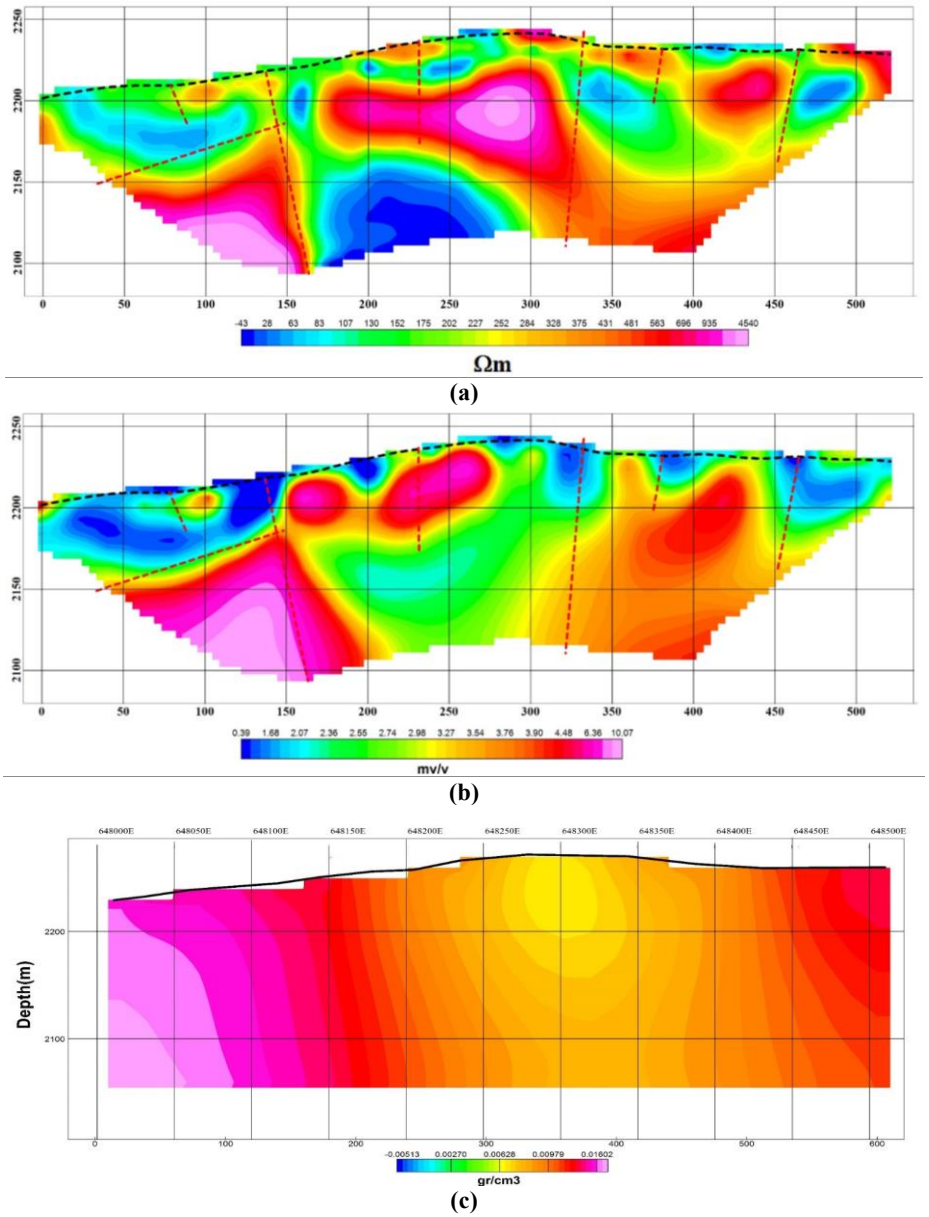

Figure 11. (a) Section results from the inversion of electrical resistivity data on the south profile, (b) section result from the inversion of inductive chargeability data on the south profile, (c) the result of modeling the data of gravity data along the southern profile.

5.3. Analysis of horizontal sections on gravity modeling

In order to better understand the structural changes as well as the extent of the porous space based on the results of the 3D gravity inversion modeling, horizontal sections of density with 50-meter intervals were prepared and drawn on the horizons of 2250, 2200, 2150, and 2100 meters (Figures 12 and 13). The faults determined in these sections were drawn based on field observations, and inference from geophysical method. According to these sections, it can be concluded that a general trend of decreasing density value can be seen in the southern part of the study area with the northwest-southeast extension, which is consistent with the results of the electrical resistivity data.

Since it is a carbonate rock unit in the studied area, and no significant difference can be seen in it, the density contrast in this area indicates a change in the sub-surface structure. The current trend of a minimum gravity anomaly in the southern part of the range can be seen in all sections, which can be considered an empty space (karst) that extends to a depth of 2100 meters (about 150 meters) in the northwest, and its depth decreases as it expands to the southeast.

The field observations and the results obtained from the geophysical data confirms that the intersection of faults that has a great depth and slope have led to the creation of karsts and blind cavities on a large surface in the region. These holes are the main feeding place for karsts, and the existing faults are channels for fluid movement, thus result in the development and expansion of karsts (Figure13). The faults picked up in the area have azimuths of 150 or 330 degrees, and the main fault of the region, which is of the thrust type, has caused the development of karsts in the region. Also there is a lot of surface evidence in the area. Even some karsts have created about 100 meters from the starting and subsidence level. By checking the maps, most of the faults in the area are deeply, and continue to depths of more than 200 meters that shows the development of karsts to higher depths.

6. Conclusions

The annual recharge of the Ravansar spring is substantial, given the high rainfall in the region, and it can supply water to several areas. Understanding the existence of a reservoir in the watershed or identifying the storage location of this spring is critical, especially in arid climates. Through extensive surveys of water transfer mechanisms, faults, regional geology, and other investigations, this work has determined that surface faults and limestone sections play a significant role in water transfer and storage. The geomorphological analysis of the Ravansar area identified many topographic depressions, that all of them are karst landforms. The geometry of each karst system is unique and different parts can be rather complex. Due to very strong lateral and vertical changes of the physical and lithological properties in karst regions, the main goal of exploration is to acquire a precise 3D geological model of the underground. Integrated geophysical methods can play an important role in building a geological model. Detailed high-definition gravimetry was successfully employed to identify natural sinkholes and karst cavity. Results from dipole-dipole and pole-dipole resistivity profiling, allowed us to define the geological boundaries of the lithological units and faults within the Ravansar area.

By means of resistivity tomography and gravity methods, we identify the direction of karst formation in the studied area. The residual gravity anomaly and the results of 3D inverse modeling show one dominant negative anomaly that were interpreted by a karst system which primarily expands in the direction of N60W, aligning with the geological information and topographical changes around known cavity. Also, the inverse electrical resistivity and induced polarization data provide a clear view of weathered soils, the distribution of weak areas or karst cavity. Several low resistivity areas were identified that shown several weak zones. The electrical resistivity imaging result proved precise and extremely efficient in delineating the karstic cavity investigation and should be taken into account when choosing an investigation technique to be used at complex geological sites. The low residual gravity has been interpreted as hitherto unknown and cavity spaces. This expands the known karst system in a southeast and northwest direction. According to the results obtained from this work, we can conclude that microgravity together with electrical resistivity tomography have proved to be effective tools for imaging sub-surface cavities in limestone at shallow depths.

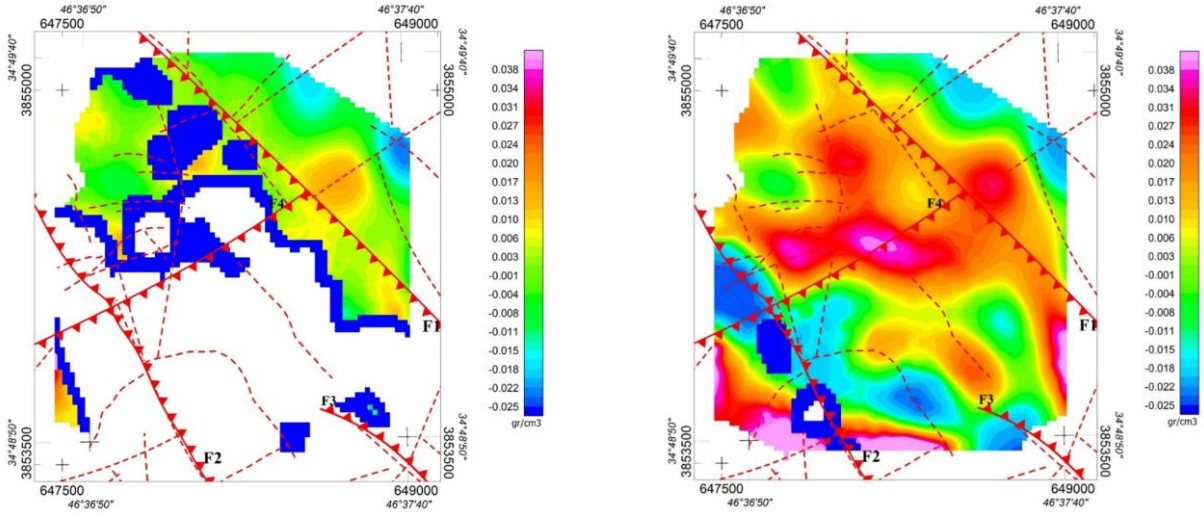

Figure12. Horizontal sections obtained from 3D inversion modeling of gravity data; Up: horizon 2250 Down, and horizon 2200

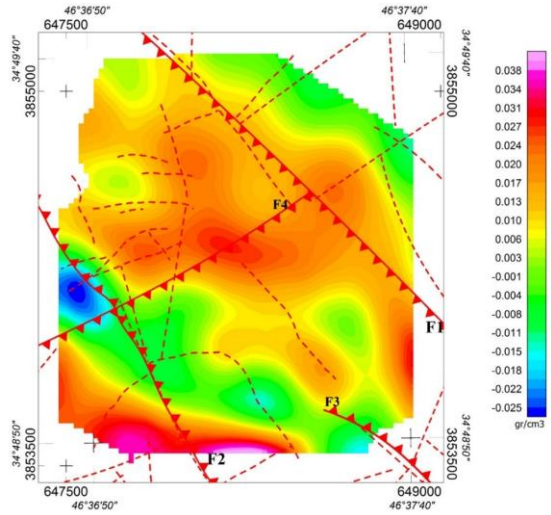

Figure13. Horizontal sections obtained from 3D inversion modeling of gravity data: Up, horizon 2150 Down, and horizon 2100.

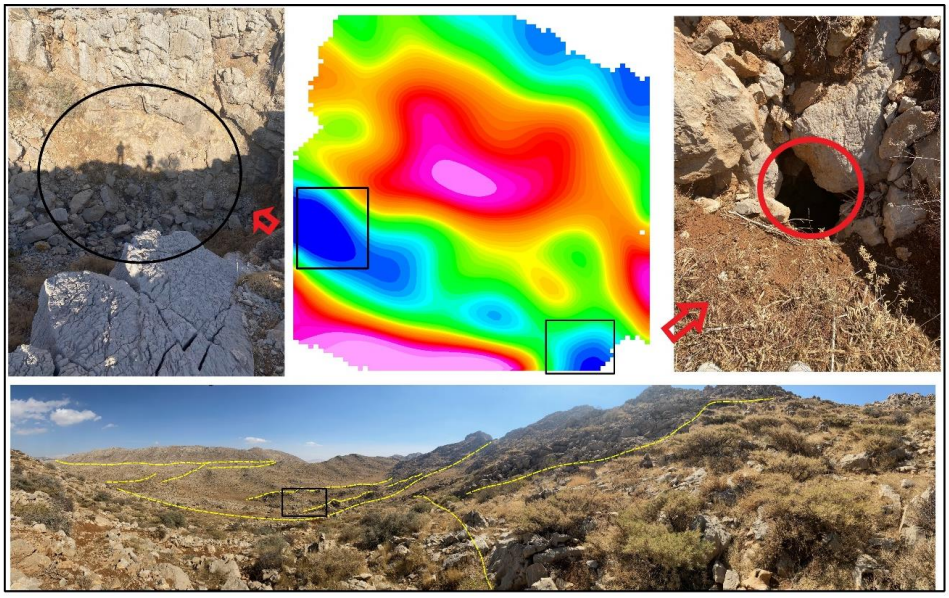

Figure 14. Effects of karstification, subsidence, pitting and faulting in the studied area.

References

[1]. Najafi, Z. and G.H. Karami. (2022). Use of GIS to Estimate Recharge and Identification of Potential Groundwater Recharge Zones in the Karstic Aquifers, West of Iran. *Advances in Geological and Geotechnical Engineering Research*, *4*(4), 1-13.

[2]. Bakalowicz, M. (2005). Karst groundwater: a challenge for new resources. *Hydrogeology journal*, *13*, 148-160.

[3]. Audra, P., et al. (2006). Cave genesis in the Alps between the Miocene and today: a review. *Zeitschrift fur Geomorphologie NF*, *50*(2), 153-176.

[4]. Auler, A.S. and Z. Stevanović. (2021). Preface: Five decades of advances in karst hydrogeology. *Hydrogeology journal*, *29*(1), 1-6.

[5]. Ford, D. and P.D. Williams. (2007). *Karst hydrogeology and geomorphology*. John Wiley & Sons.

[6]. Lubang, J., H. Liu, and R. Chen. (2023). Combined Application of Hydrogeological and Geoelectrical Study in Groundwater Exploration in Karst-Granite Areas, Jiangxi Province. *Water*, *15*(5), 865.

[7]. De Waele, J., et al. (2011). Geomorphology and natural hazards in karst areas: a review. *Geomorphology*, *134*(1-2), 1-8.

[8]. Gutiérrez, F., et al. (2014). A review on natural and human-induced geohazards and impacts in karst. *Earth-Science Reviews*, *138*, 61-88.

[9]. Cardarelli, E., et al. (2010). Electrical resistivity and seismic refraction tomography to detect buried cavities. *Geophysical prospecting*, *58*(4), 685-695.

[10]. De Giorgi, L. and G. Leucci. (2014). Detection of hazardous cavities below a road using combined geophysical methods. *Surveys in Geophysics*, *35*, 1003-1021.

[11]. Chico, R.J. (1964). Detection of caves by gravimetry. *International Journal of Speleology*, *1*(1), 11.

[12]. Butler, D.K. (1984). Microgravimetric and gravity gradient techniques for detection of subsurface cavities. *Geophysics*, *49*(7), 1084-1096.

[13]. Castillo, R.R. and R.R. Gutiérrez. (1992). Resistivity identification of shallow mining cavities in Real del Monte, México. *Engineering Geology*, *33*(2), 141-149.

[14]. McGrath, R., et al. (2002). Integrated high-resolution geophysical investigations as potential tools for water resource investigations in karst terrain. *Environmental Geology*, *42*, 552-557.

[15]. Jia, X., et al. (2022). Application of the high-density resistivity method in detecting a mined-out area of a quarry in Xiangtan City, Hunan Province. *Frontiers in Environmental Science*, *10*, 1068956.

[16]. El-Qady, G., et al. (2005). Imaging subsurface cavities using geoelectric tomography and ground-penetrating radar. *Journal of cave and karst studies*, *67*(3), 174-181.

[17]. Leucci, G. and L. De Giorgi. (2005). Integrated geophysical surveys to assess the structural conditions of a karstic cave of archaeological importance. *Natural hazards and earth system sciences*, *5*(1), 17-22.

[18]Carpenter, P.J. and D.W. Ekberg. (2006). Identification of buried sinkholes, fractures and soil pipes using ground-penetrating radar and 2D electrical resistivity tomography. Proceedings of the 2006 highway geophysics-NDE conference,

[19]. Leucci, G. and S. Negri. (2006). Use of ground penetrating radar to map subsurface archaeological features in an urban area. *Journal of Archaeological Science*, *33*(4), 502-512.

[20]. Radulescu, V., et al. (2007). GEOELECTRICAL STUDY FOR DELINEATING UNDERGROUND CAVITIES IN KARST AREAS. *GeoEcoMarina*, *13*(1).

[21]Vargemezis, G., et al. (2007). Application of Electrical Resistivity Tomography in Monitoring Recycled Water Injection. Near Surface 2007-13th EAGE European Meeting of Environmental and Engineering Geophysics,

[22]. Abu-Shariah, M.I. (2009). Determination of cave geometry by using a geoelectrical resistivity inverse model. *Engineering Geology*, *105*(3-4), 239-244.

[23]. Lazzari, M., A. Loperte, and A. Perrone. (2010). Near surface geophysics techniques and geomorphological approach to reconstruct the hazard cave map in historical and urban areas. *Advances in Geosciences*, *24*, 35-44.

[24]. Pánek, T., et al. (2010). Gravitationally induced caves and other discontinuities detected by 2D electrical resistivity tomography: Case studies from the Polish Flysch Carpathians. *Geomorphology*, *123*(1-2), 165-180.

[25]. Kovacic, G. and N.x. Nataša Ravbar. (2010). Extreme hydrological events in karst areas of Slovenia, the case of the Unica River basin. *Geodinamica Acta*, *23*(1-3), 89-100.

[26]. Valois, R., et al. (2010). Karstic morphologies identified with geophysics around Saulges caves (Mayenne, France). *Archaeological Prospection*, *17*(3), 151-160.

[27]. Gambetta, M., et al. (2011). Determining geophysical properties of a near-surface cave through integrated microgravity vertical gradient and electrical resistivity tomography measurements. *Journal of cave and karst studies*, *73*(1), 11-15.

[28]. Abd El Aal, A. (2017). Identification and characterization of near surface cavities in Tuwaiq Mountain Limestone, Riyadh, KSA,"detection and treatment". *Egyptian Journal of Petroleum*, *26*(1), 215-223.

انجمن مهندسی معدن ایران
نشریه مهندسی معدن و محیط زیست
نشانی نشریه: www.jme.shahroodut.ac.ir
دانشگاه صنعتی شاهرود

آشکارسازی ویژگی‌های کارست‌ها با تلفیق روش‌های ژئوفیزیکی، مطالعه موردی شمال غرب روانسر

حمیدرضا باغزندانی[1]، حمید آقاجانی[1*] و غلامحسین کرمی[2]

۱. دانشکده مهندسی معدن، نفت و ژئوفیزیک، دانشگاه صنعتی شاهرود، شاهرود، ایران
۲. دانشکده علوم زمین، دانشگاه خوارزمی، کرج، ایران

اطلاعات مقاله

تاریخ ارسال: ۲۰۲۴/۰۸/۲۶
تاریخ داوری: ۲۰۲۴/۱۰/۰۸
تاریخ پذیرش: ۲۰۲۴/۱۰/۲۰

DOI: 10.22044/jme.2024.14984.2855

کلمات کلیدی

تشخیص حفرات
میکروگرانی
مقاومت الکتریکی
پلاریزاسیون القایی
کارست

چکیده

کارست‌ها منابع مهم آب‌های زیرزمینی هستند و تعیین حجم و کیفیت آب آن‌ها بسیار مهم است. چشمه کارستی روانسر در استان کرمانشاه یک منبع و سفره آبی بزرگ با ذخیره قابل توجه آب در منطقه است. منشای آبی این چشمه واحدهای کربناته متعلق به دوره کرتاسه شمال غرب آن است که متاثر از حرکات زمین ساختی و گسل‌های ناشی از چین‌خوردگی زاگرس است. در این کار از روش‌های ژئوفیزیکی میکروگرانی، مقاومت الکتریکی و پلاریزاسیون القایی برای شناسایی میزان توسعه کارست در واحدهای کربناته (سنگ آهک) استفاده شده است. مقادیر کمینه آنومالی گرانی باقی‌مانده با پدیده کارستی شدن ارتباط مستقیم و مقادیر مقاومت ویژه الکتریکی و قطبش القایی نیز به توسعه کارستی شدن و سیال درون آن وابسته است. دو دسته داده گرانی برداشت شده روی یک شبکه و داده الکتریکی برداشت شده روی دو پروفیل با آرایه دوقطبی-دوقطبی و قطبی-دوقطبی مورد استفاده قرار گرفته است. مدل‌سازی وارون داده‌های الکتریکی و گرانی با استفاده از الگوریتم دوبعدی به روش کمترین مربعات با قید هموارساز انجام شده است. براساس پردازش و مدل‌سازی سه بعدی داده‌های گرانی؛ نه تنها حفره‌ها و فضاهای خالی بزرگ شناسایی شدند، بلکه ساختارهای زیرسطحی و توسعه پدیده کارستی شدن در سنگ‌های کربناته منطقه مورد مطالعه بارز و آشکار شده‌اند. مهم‌ترین نتیجه از بررسی میدانی، بازشدن فروچاله‌های بزرگ و فضاهای خالی و فروافتاده زیرسطحی است که با مقادیر کم گرانی مرتبط است که پیش‌تر ناشناخته بوده و از سطح زمین قابل دسترس نبوده‌اند. نتایج بدست آمده نشان می‌دهد، گسترش عمقی کارست‌ها و کارست‌های پر شده از رسوبات، که در فروچاله‌های سطحی، حفره‌ها و سیستم‌های توسعه یافته کارست دیده می‌شود، با شرایط زمین‌شناسی و تکتونیکی منطقه مطابقت دارد. بررسی‌های ژئوفیزیکی و مشاهدات صحرایی نشان می‌دهد که چاله‌ها و کارست‌های منطقه مرتبط با پدیده‌های تکتونیکی و گسلش بوده و مجاری انتقال و عبور آب از بخش‌های بالادست به سمت چشمه کارستی روانسر هستند.

نویسنده مسئول مکاتبات: haghajani@shahroodut.ac.ir (ح. آقاجانی)